ADVANCED FUNCTIONAL MATERIALS
www.afm-journal.de

Materials Views
www.MaterialsViews.com

The Poisson Ratio in $CoFe_2O_4$ Spinel Thin Films

*Michael Foerster, Milko Iliev, Nico Dix, Xavier Martí, Mykhailo Barchuk, Florencio Sánchez, and Josep Fontcuberta**

The response of epitaxial $CoFe_2O_4$ thin films to biaxial compressive stress imposed by $MgAl_2O_4$ and $SrTiO_3$ single crystalline substrates is studied using X-ray diffraction and Raman spectroscopy. It is found that the Poisson ratio ν signals a non-auxetic behavior and depends on the substrate used. The Raman modes show an increase in frequency when increasing compressive strain by reducing film thickness; this is due to the shrinking of the unit cell volume. Such behavior is in qualitative agreement with recent ab initio calculations, although the measured values are significantly smaller than predictions. In contrast, the measured Poisson ratio is found to be in good agreement with expectations based on general arguments of atomic packing density. Possible guidelines for searching auxetic response in materials with spinel structure are discussed.

1. Introduction

The Poisson ratio (ν) of solids is a measure of the resistance of a material to distort under a mechanical stress rather than to alter its volume. The Poisson ratio defined by $\nu = -\varepsilon_t/\varepsilon_l$, is related to the ratio of the longitudinal deformation ε_l by a load and the resulting transversal deformation ε_t. It describes, in a narrow numerical range ($-1 < \nu < 1/2$ for isotropic materials), the different behavior of solids, from rubber to ceramics, as well as colloidal crystals and critical fluids. For $\nu > 0$, the material expands in a direction transverse to a (compressive) load and the volume is preserved for $\nu = 1/2$ (i.e., an ideal rubber). In the more uncommon case of $\nu < 0$, the materials contracts in the transverse direction to the load ("anti-rubber" as they respond to a load opposite to rubber).[1] This observation emphasizes that the Poisson ratio collects fundamental characteristics of the material, either of the microstructure or the interatomic interactions and bonds in solids. For instance: whereas very dense and weakly compressible materials have $\nu \approx 1/2$, more open structures, such as zeolites or cork, may lead to reduced ($\nu \approx 0$) or even negative ($\nu < 0$) Poisson ratios.[2]

The Poisson ratio is receiving renewed attention due to recent progress in understanding the rich information it contains[3] and the recognition that exotic materials, such as those having $\nu < 0$ (so-called *auxetic*),[4] are much more abundant that previously thought.[5] Although long believed that auxetic behavior required foam-like or honeycomb structures, the observation that about 70% of body-centred cubic (bcc) elemental metals have negative Poisson ratios along the [110] direction and the suggestion of an enlightening atomistic picture describing the observed phenomena has stimulated a new view on this topic.[3] This observation also highlights the fact that in anisotropic materials, the Poisson ratio can differ strongly depending on the direction.

Auxetic single-crystalline alloys are of relevance in some high-tech applications as structural materials.[6] However, auxetic response could have an even more dramatic impact on the functional properties of materials as it signals strong, non-volume conserving, changes of interatomic distances and bonding angles in solids. In the case of ferroelectric perovskite $BaTiO_3$, for instance, it has been shown that the soft-mode accompanying the paraelectric–ferroelectric transition is accompanied by an auxetic minimum of the Poisson ratio.[7]

In thin films, epitaxial stress due to substrate–film structural mismatch most commonly induces strains in the films that could greatly modify their properties. Strain effects are well documented in materials having a perovskite structure, such as $SrTiO_3$ in which ferroelectricity can be induced by strain,[8] or $BaTiO_3$ in which the ferroelectric phase transitions is known to be largely dependent on strain.[9,10] Strain effects are particularly relevant in magnetic oxide thin films, where the superexchange or double-exchange magnetic interactions are strongly sensitive to the metal–oxygen–metal bond angle and distances.[11,12] Magnetic oxides thin films having either perovskite (ABO_3) or spinel (AB_2O_4) structures are being intensively studied due to their potential applications in several advanced technology fields, e.g., spintronics. Whereas strain effects on (ferro)magnetic or (anti)ferromagnetic perovskites[13,14] are well documented, the

Dr. M. Foerster, N. Dix, Dr. F. Sánchez,
Prof. J. Fontcuberta
Institut de Ciència de Materials de Barcelona
(ICMAB-CSIC),
Campus UAB, 08193 Bellaterra, Spain
E-mail: fontcuberta@icmab.es
Dr. M. Foerster
Institut für Physik
Johannes Gutenberg-Universität Mainz
Staudinger Weg 7, 55099 Mainz, Germany
Prof. M. Iliev
Texas Center for Superconductivity and Department of Physics
University of Houston
Houston, TX 77204-5002, USA
Dr. X. Martí, M. Barchuk
Department of Condensed Matter Physics
Faculty of Mathematics and Physics
Charles University
Ke Karlovu 5, 121 16 Prague 2, Czech Republic

DOI: 10.1002/adfm.201200257

effects of epitaxial stress on the structure of magnetic spinels are not yet well understood.[15–18]

From first view, one could anticipate that stress effects on unit-cell metrics and bond topology could be more relevant in oxide-based open structures, such as the spinel, than in the more densely packed perovskite structure. Probably for this reason, the Poisson ratio of spinel-based thin films has recently received much attention.[19–21] Somehow in agreement with views just described, it has been reported that thin films of $CoFe_2O_4$, a prototypical spinel-ferrite oxide, grown on a perovskite ($SrTiO_3$) substrate, could be auxetic, i.e., display a negative Poisson ratio ($\nu < 0$).[19] Interestingly, it has been proposed that this effect results from the existence of some particular honeycomb-like 3D network of meta-oxygen bonds in the spinel structure and argued that $\nu < 0$ could thus be a genuine characteristic of the spinels with profound impact on several functional properties, namely magnetic anisotropy and magnetostriction. Recently, Ziese[21] determined the Poisson ratio in (spinel) Fe_3O_4 thin films grown on isostructural $MgAl_2O_4$ substrates and concluded that Fe_3O_4 is not auxetic. However, results from those studies cannot be safely compared as both films and substrates were different and it is known that strain relaxation in thin films, and thus cell parameters, may differ depending on the precise growth mode and growth conditions. On the other hand, recent first-principle calculations of strain effects in spinel ferrites thin films[22] predicted $\nu > 0$, thus calling for new efforts on this topic. Prospects of new applications of ferrimagnetic spinels in spintronics urge such studies.[23]

Here we have revisited this question by performing comprehensive structural and Raman scattering studies on epitaxial thin films of $CoFe_2O_4$ (CFO) grown on $SrTiO_3$(STO) and $MgAl_2O_4$ (MAO) substrates. CFO is a robust room-temperature insulating ferrimagnet that has received attention as a possible spin filter.[24–29] As STO and MAO have different cell parameters and structures (perovskite and spinel respectively), the choice of these substrates allows the exploration of distinct stresses and growth modes and their influence on the strain state of CFO epitaxial films. For completeness, films grown at very different growth rates (3 nm min^{-1} by pulsed laser deposition (PLD) and 0.1 nm min^{-1} by radio frequency (RF) sputtering) are also compared.

We will show that for all CFO films a positive Poisson ratio ($\nu > 0$) is observed. However, epitaxial stress largely deforms the unit cell in a non-volume preserving manner, thus impacting the lattice dynamics in a rather unexpected way, as demonstrated by the Raman data. We argue that the non-auxetic behavior is in agreement with a basic understanding of the trend of Poisson ratio in solids, namely the determining role of the atomic packaging density, and we will show that Raman data provides a unique insight into stress effects in these CFO thin films.

2. Experimental Section

CFO films of thicknesses (t) ranging from 4 up to 150 nm were grown simultaneously on (001)STO and (001)MAO substrates from CFO stoichiometric targets. Two different deposition techniques were employed: i) pulsed laser deposition using a KrF laser with a 1.6 J cm^{-2} fluence and a repetition rate of 5 Hz at T = 500 °C and oxygen pressure of 0.1 mbar, and, ii) RF-sputtering with an Ar/O_2 ratio of 10:1, and a total pressure of 0.333 mbar at 500 °C. The growth rates were around 3 nm min^{-1} for PLD and around 0.1 nm min^{-1} for RF sputtering. The thickness of the films was determined by X-ray reflectometry.

STO and MAO substrates both have a cubic structure and their respective cell parameters are: $2a_{STO}$ = 7.81 Å and a_{MAO} = 8.083 Å. Bulk CFO is also cubic (a_{CFO} = 8.392 Å). Therefore, the lattice mismatches between the film and substrates, here defined as $f = (a_{film}-a_{subs})/a_{film}$) are: f_{MAO} = +3.6% and f_{STO} = + 6.9%, and both substrates impose a compressive in-plane stress on the CFO films.

The CFO film out-of-plane (OOP) lattice parameters were determined from $\theta/2\theta$ scans using a Siemens D-5000D diffractometer and Cu-$K_{\alpha1,2}$ radiation. The positions of the substrate ($K_{\alpha1}$ and $K_{\alpha2}$) reflections [(004) and (008) for MAO; (002) and (004) for STO] were used for internal angular calibration by assuming the bulk values of the substrates lattice constants (8.083 and 3.905 Å, respectively). The typical experimental error of CFO out-of-plane cell parameter (c) is estimated to be ±0.004 Å.

Using a Bruker AXS, model D8 Advance diffractometer equipped with a GADDS area detector, intensity maps (Q-plots) around the CFO (115) reflection were performed to determine the in-plane (IP) lattice constant of the CFO films. The in- and out-of-plane momentum transfer Q_{IP}, Q_{OOP} were calculated from the experimental 2θ and ω angles, with offset ω angles determined from the closest substrate reflection (for MAO (115), and STO (113)). The in- and out-of-plane lattice constants (a and c) of CFO were calculated from the position center (Q_{IP}, Q_{OOP}) of the measured intensity distribution.

Polarized Raman spectra were measured with 488 or 515 nm excitation, at room temperature, using a T64000 spectrometer equipped with a microscope. The first letter and second letter in scattering configuration notations XX and XY denote, respectively, the polarization of incident and scattered light with respect to the crystallographic directions. For the spectra presented below, X and Y correspond to $[100]_c$ and $[010]_c$ cubic directions, respectively. The raw spectra were superpositions of spectra of the CFO film and substrate. The substrate signal was eliminated by measuring the substrate spectra in the same scattering configuration and subtracting them from the combined spectra.

3. Results

In **Figure 1** we show a zoom of the $\theta/2\theta$ scans of CFO-PLD films of various thicknesses grown on MAO (CFO-PLD//MAO) and STO (CFO-PLD//STO). The vertical line indicates the position of the (004) reflection of bulk CFO. These figures reveal that the (004) reflection of the thinner films are well shifted towards smaller angles indicating that their c-axes are expanded compared to bulk CFO. This is the expected trend for a non-auxetic material under compressive in-plain epitaxial stress. As expected, increasing the thickness leads to structural relaxation. In the case of (CFO-PLD//MAO) the bulk value is recovered at $t \approx 100$ nm, whereas in the case of (CFO-PLD//STO), the larger structural mismatch drives an earlier relaxation.

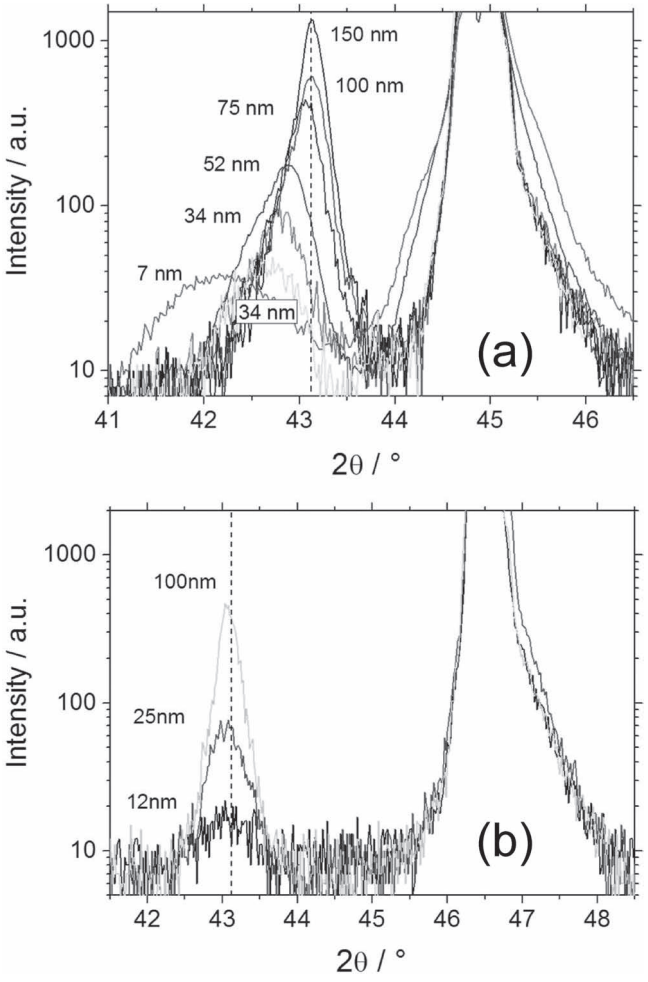

Figure 1. X-ray diffraction $\theta/2\theta$ scans of the $CoFe_2O_4$ (004) reflection for different layers (prepared by PLD) with thickness as indicated: a) on $MgAl_2O_4$ substrates and b) on $SrTiO_3$ substrates. The vertical lines indicate the expected position for the out-of-plane parameter of bulk $CoFe_2O_4$. Peaks to the right are due to the corresponding substrate reflection: (004) for $MgAl_2O_4$ and (002) for $SrTiO_3$.

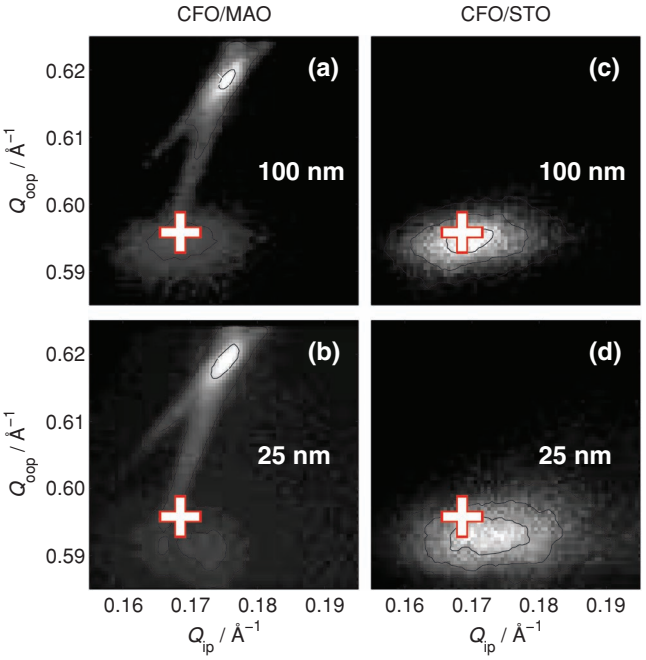

Figure 2. Reciprocal space maps around the $CoFe_2O_4$ (115) reflection: intensity vs. in-plane Q_{ip} and out-of-plane momentum transfer Q_{oop}: a) $CoFe_2O_4$ (25 nm) on $MgAl_2O_4$, and, b) $CoFe_2O_4$ (100 nm) on $MgAl_2O_4$. Corresponding data for $CoFe_2O_4$ films on $SrTiO_3$ substrates are shown for thicknesses of: c) 25 nm, and, d) 100 nm. The expected peak position for $CoFe_2O_4$ bulk single crystals is indicated by a cross.

Q-plots around the (115) reflection of CFO films of different thicknesses grown on STO and MAO are shown in **Figure 2**. The crosses in these plots indicate the (Q_{IP}, Q_{OOP}) position expected for bulk CFO. The data clearly show that the reflection for the thinnest film on MAO is well shifted (Figure 2b) towards larger Q_{IP}, thus indicating that the in-plane cell parameter (*a*-axis) is shortened; this is the expected behavior for in-plane compressively stressed films. At the same time, and in agreement with the $\theta/2\theta$ scans of Figure 1a, the corresponding Q_{OOP} maxima occurs at smaller *Q*-values than expected for bulk, thus indicating an expansion of the *c*-axis. As shown by the data in Figure 2a, when film thickness increases, the in-plane shift is reduced and the position of the (115) reflection closely approaches the bulk value. In comparison, for CFO films grown on STO substrates (Figure 2c,d), the lattice parameters approach bulk values at much lower thickness (for instance t = 25 nm in Figure 2d), thus indicating a faster relaxation.

Figure 3a,b show the (*a*,*c*) cell parameters of all CFO-PLD//MAO films grown in two runs (series A and B; open and solid squares, respectively). Solid lines indicate the corresponding bulk values. Data in these plots clearly reveal that the substrate-induced stress compresses the in-plane CFO cell parameter while expanding the out-of-plane parameter. However, as shown in Figure 3c (solid squares), the unit-cell volume is not preserved but reduces when reducing film thickness. In Figure 3a we also include the *c*-axis values (rhombi) of CFO films of various thicknesses, grown by RF-sputtering (CFO-RF//MAO). In agreement with data of the (CFO-PLD//MAO) series, and in spite of larger data dispersion (films were grown in different runs), all *c*-axis values are expanded compared to bulk.

In Figure 3a,c we include data for CFO films of various thicknesses grown on STO, either by PLD or RF-sputtering: CFO-PLD//STO and CFO-RF//STO respectively. One immediately notices in Figure 3a that for the thinnest films the *c*-axis is expanded compared to the bulk, which is the same trend as shown by films on MAO. A difference is that films on STO (irrespectively of the growth technique) relax faster, already approaching the bulk value at about 40–50 nm. This behavior is as expected from the larger mismatch in CFO//STO (+6.9%) than in CFO//MAO (+3.6%), which tends to produce plastic defects facilitating relaxation of epitaxial stress. Consistently with the variation of the out-of-plane parameter, the *a*-axis is compressed in thinnest CFO//STO films and rapidly relaxes towards bulk values (Figure 3b). The final observation, collected in Figure 3c, is that also in the CFO//STO films, the unit-cell volume shrinks when reducing the film thickness. All data

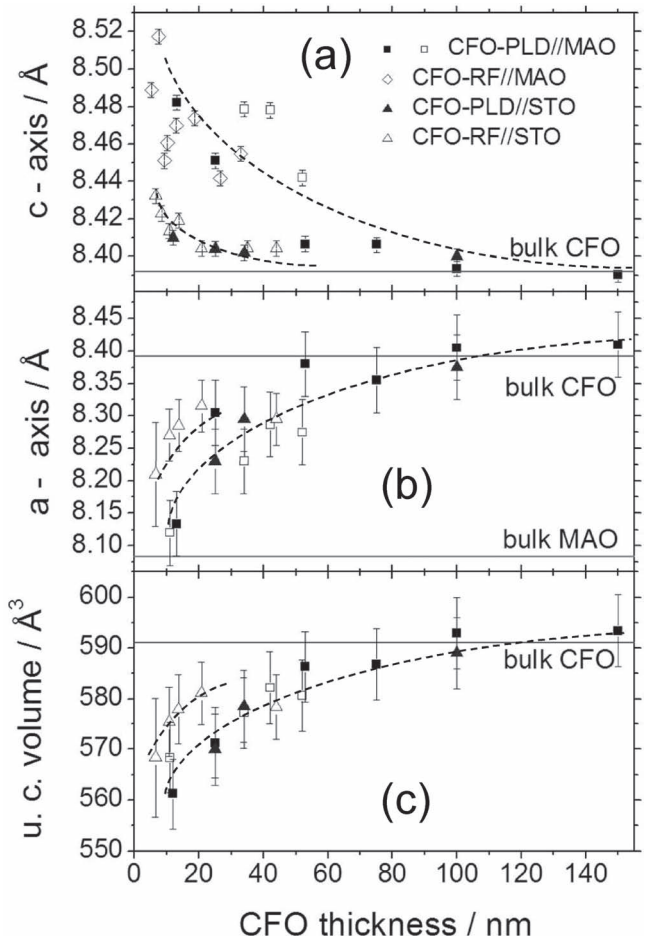

Figure 3. Lattice parameters for $CoFe_2O_4$ thin films calculated from x-ray diffraction data as function of the film thickness for different sample series as indicated: a) out-of-plane parameters calculated from the (004) and (008) peak positions in 2-circle X-ray diffraction pattern as shown in Figure 1, b) in-plane lattice parameter calculated from the centre of the intensity distribution in reciprocal space maps as shown in Figure 2, and c) calculated unit cell volume assuming a tetragonal distorted unit cell from parameters shown in panel (a) and (b). Horizontal lines correspond to $CoFe_2O_4$ bulk single crystal values. Dashed lines serve as guides to the eye.

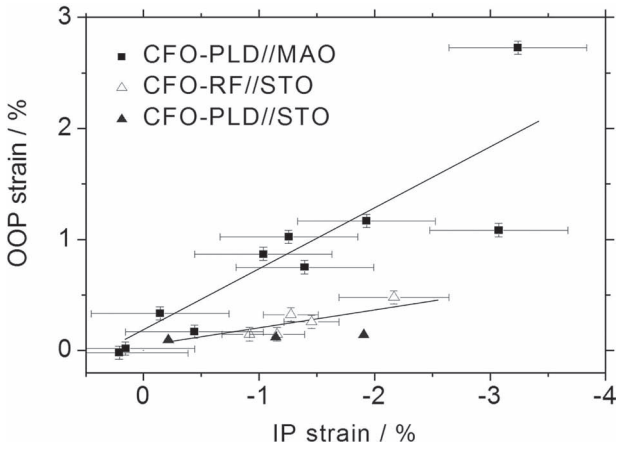

Figure 4. Strain diagram for epitaxially strained $CoFe_2O_4$ thin films: the out-of-plane strain vs. in-plane strain from data in Figure 3. The different apparent Poison ratios of samples grown on $MgAl_2O_4$ compared to those grown on $SrTiO_3$ are indicated by straight lines.

reported in Figure 3a–c show that both CFO//MAO and CFO//STO display in-plane compression and out-of-plain expansion and thus all films have a positive Poisson ratio ($\nu > 0$).

For an epitaxial film under 2D stress, the apparent Poisson ratio ν^* is given by $\nu^* = -\varepsilon_{oop}/\varepsilon_{ip} = 2\nu/(1-\nu)$;[30] the strains ε_{oop} and ε_{ip} are calculated from the out-of-plane and in-plane (c, a) cell parameters of the film and the corresponding bulk values ($c^b = a^b = a_{CFO}$) as $\varepsilon_{oop} = (c - c^b)/c^b$ and $\varepsilon_{ip} = (a - a^b)/a^b$, respectively. Therefore values of ν^* for CFO can be obtained from plots of ε_{oop} vs. ε_{ip}, as shown in **Figure 4**, where data for CFO-PLD//MAO and CFO//STO films of various thicknesses are included. Figure 4 indicates that films grown on either MAO or STO display a roughly linear variation of ε_{oop} on ε_{ip} thus indicating that both series of films have well-defined and positive $\nu^*, \nu > 0$ values. A linear fit of the $\varepsilon_{oop}(\varepsilon_{ip})$ data gives ν^*(CFO//MAO) ≈ 0.57 and ν^*(CFO//STO) ≈ 0.27. These positive Poisson ratios reflect that under compressive in-plane stress, the out-of-plane cell parameters doubtlessly expand, but not as much as required to preserve the unit cell volume; this would (in the limit of small strain values) require $\nu^* = 2$, that is: $\nu = 0.5$. Remarkably the Poisson ratio derived here and the value reported for strained Fe_3O_4//MAO films[21] ($\nu^* \approx 0.3$) roughly agree, thus suggesting that they reflect the actual elastic properties of epitaxial spinel thin films. The Poisson ratio of CFO//STO is found to be significantly smaller than that of CFO//MAO; the faster structural relaxation associated with the larger mismatch in CFO//STO films and the concomitant pattern of plastic defects may be responsible for this reduced Poisson ratio. In fact, from the elastic constant of single crystalline CFO (C_{11} = 257 GPa; C_{12} = 150 GPa)[31] it follows that $\nu^* = 1.16$, which is in close agreement with recent theoretical estimations.[22]

The data presented above indicate that in responding to epitaxial stress CFO changes its lattice distances and unit cell volume. These observations are relevant because they anticipate a remarkable effect on the phonon spectrum. In **Figure 5** we show illustrative room-temperature Raman data collected on CFO-PLD//MAO films of series A and B, of different thicknesses. In Figure 5a we show data collected using parallel *XX* configuration and a laser wavelength of 515 nm; data in Figure 5b were collected using crossed *XY* configuration and a laser wavelength of 488 nm. The position of the Raman peaks together with their polarization dependence allows distinct modes to be assigned, as described elsewhere.[32] We will mention here that due to the local short range ordering of Co^{2+} and Fe^{3+} at the octahedral sites, the Raman spectrum of CFO is richer than expected for an ideal spinel structure of Fd-3m symmetry where one expects only two modes (A_{1g} + E_g) in the *XX* spectrum and only three F_{2g} modes in the *XY* spectrum. The Raman peaks corresponding to these modes in bulk CFO are at 210 cm^{-1} (F_{2g}, *XY*), 305 cm^{-1} (E_g, *XX*), 466 cm^{-1} (F_{2g}, *XY*), 577 cm^{-1} (F_{2g}, *XY*), and 695 cm^{-1} (A_{1g}, *XX*); the main atomic motions are shown in **Figure 6**. As seen, these motions are neither purely in-plane nor purely along the *c*-axis but instead are in general along the cubic space diagonals.

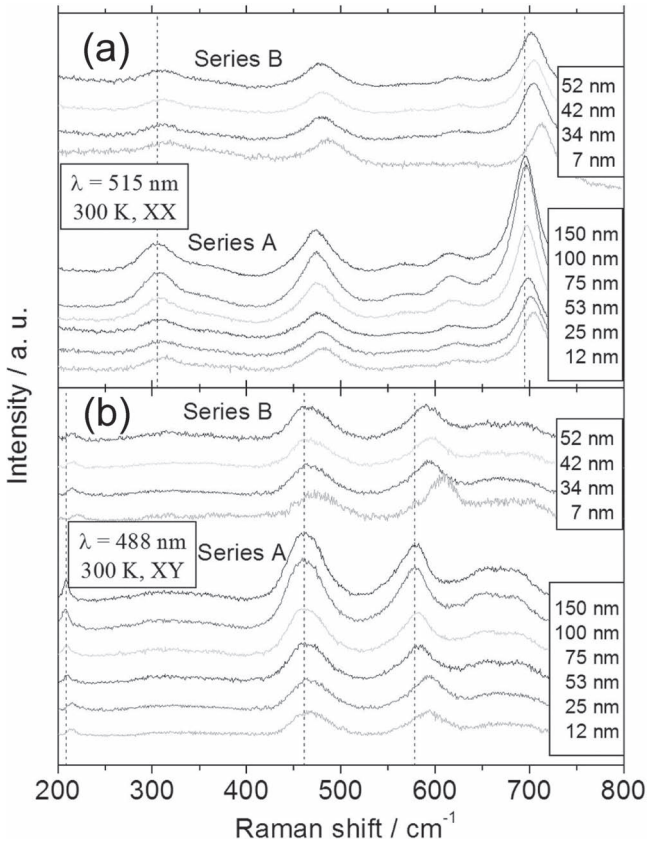

Figure 5. Illustrative Raman data for $CoFe_2O_4$ films of different thickness grown by PLD on $MgAl_2O_4$ substrates. The substrate contribution has been subtracted. Data obtained in different scattering configuration (*XX* and *XY*) and using different laser wavelength are shown. Vertical dashed lines indicate the peak position for the thickest CFO film.

Next, the focus is on the shifts of the Raman modes when varying the films thickness. It is apparent that the position of the Raman modes depends on film thickness, thus reflecting the strain state of the films. This is illustrated in **Figure 7** where the position of the A_{1g} mode at 712–695 cm^{-1}, measured using different laser wavelengths, is plotted versus the film thickness. Moreover, the data in this plot indicate that films of series A and B – although having the same thickness – have a distinct phonon pattern, which thus reflects different strain states resulting from fine distinct details of the growth mode. In fact, a corresponding difference between series A and B samples is also found by a close inspection of the OOP lattice constants in Figure 3a, confirming that Raman spectroscopy indeed serves as a sensitive tool to investigate the CFO film strain state. But of more interest here is the observation that when increasing the film thickness, there is a red shift of the Raman mode, thus indicating a softening of the restoring force of the corresponding oscillator. A similar trend is observed for all Raman modes in Figure 5.

At first sight, the data in Figure 5 and 7 are intriguing. It was shown in Figure 3a that when increasing film thickness, the *c*-axis reduces; therefore the data in Figure 3a indicate that the dependence of the phonon frequency ω on thickness cannot be explained by the simple variation of the OOP cell parameter. Indeed, if for the A_{1g} mode $\omega \sim 1/d^n$, where d is the length of the Fe–O bonds of the FeO_4 tetrahedra in CFO and $n = 3/2$,[33] then one should expect a blue-shift of the Raman mode instead of a red-shift, as the diagonal length would increase for a volume conserving tetragonal distortion. As a similar red-shift is observed for all modes when increasing thickness, the *c*-axis contraction alone upon increasing thickness cannot account for the observed behavior. It follows that the combined effect of the variations of *c*-axis (expansion) and *a*-axis (compression) with decreasing film thickness should be explicitly considered. A relevant insight is derived from data in Figure 3c, which shows that the unit cell volume expands with increasing film thickness; therefore the average distances $\langle d \rangle = \langle M–O \rangle$ should increase and thus the corresponding Raman frequency should soften (reduce ω); this is in agreement with experimental data.

Even though, as we have shown in Figure 3 and 4, the *c*-axis contraction and *a*-axis expansion are directly linked via the Poisson ratio, it may be suspected that the experimental data for both series A and B, which taken together result in a non-monotonous thickness dependence $\omega(t)$, may be univocally described by an expression $\omega(c) = \omega\{c,a(c)\}$, where $a(c)$ is given by the Poisson ratio. We choose here the OOP lattice parameter *c* to represent the strain state as it is experimentally determined more accurately than the IP *a* value.

In **Figure 8**, we show the dependencies of all Raman modes on the *c*-axis length of the corresponding films. Data in these plots indeed confirm that $\omega(c)$ varies monotonically for all films. Moreover a simple power-law dependence $\omega(c) = \omega_0 (1 + Z(c–c_0)\beta)$ can be used to describe the observed dependence. Excellent fits can be obtained (solid lines through the data) using the best-fit parameters (Z, β) shown in **Table 1**. In Figure 8, no difference between the samples of the A and B series is visible, i.e., the description $\omega(c)$ works likewise for both types of samples, implying that the CFO film thickness has no direct influence on ω apart from its impact on the strain state.

Maybe more transparent than this empirical power law dependence could be the recognition that, as the discussed phonon modes involve movements along the unit cell diagonal, the diagonal length $d_D = (2a^2 + c^2)^{1/2}$ of the tetragonal unit cell could be used to estimate the characteristic average bond length $\langle d \rangle \approx d_D$. As shown by Iliev et al.[33] $\omega(\langle d \rangle)/\omega(\langle d_0 \rangle) = \langle d_0 \rangle^{3/2}/\langle d \rangle^{3/2}$ where $\langle d_0 \rangle$ is the corresponding value for bulk (relaxed) material; in other words $\omega(d_D)/\omega_0 = d_{D0}{}^{3/2}/d_D{}^{3/2}$ should be a straight line, where $d_{D0} = a_0$ℭ is the diagonal length of the undistorted bulk-like CFO unit cell. (It should be noted, however, that for our data another characteristic length $d_V = V^{1/3} = (a^2c)^{1/3}$ gives very similar values: $d_V \approx d_D$. Therefore a very similar description may be obtained based on d_V instead of d_D).

The relation between the normalized frequency $\omega(d_D)/\omega_0$ and the factor $d_{D0}{}^{3/2}/d_D 3/2$ is shown in the insets of Figure 8, where it can be appreciated that this simple model describes rather accurately the observed shifts of the Raman modes at least for three of the modes. The two F_{2g} modes (*XY* 577 cm^{-1} and *XY* 210 cm^{-1}) for which this description does not work are the same for which the parameter Z in the fits described above is much bigger than for the other three. To what extent this discrepancy is related to the precise nature of these modes, their particular dependencies on *a* and *c* and their modification upon strain, cannot be inferred from the present data. Anyhow

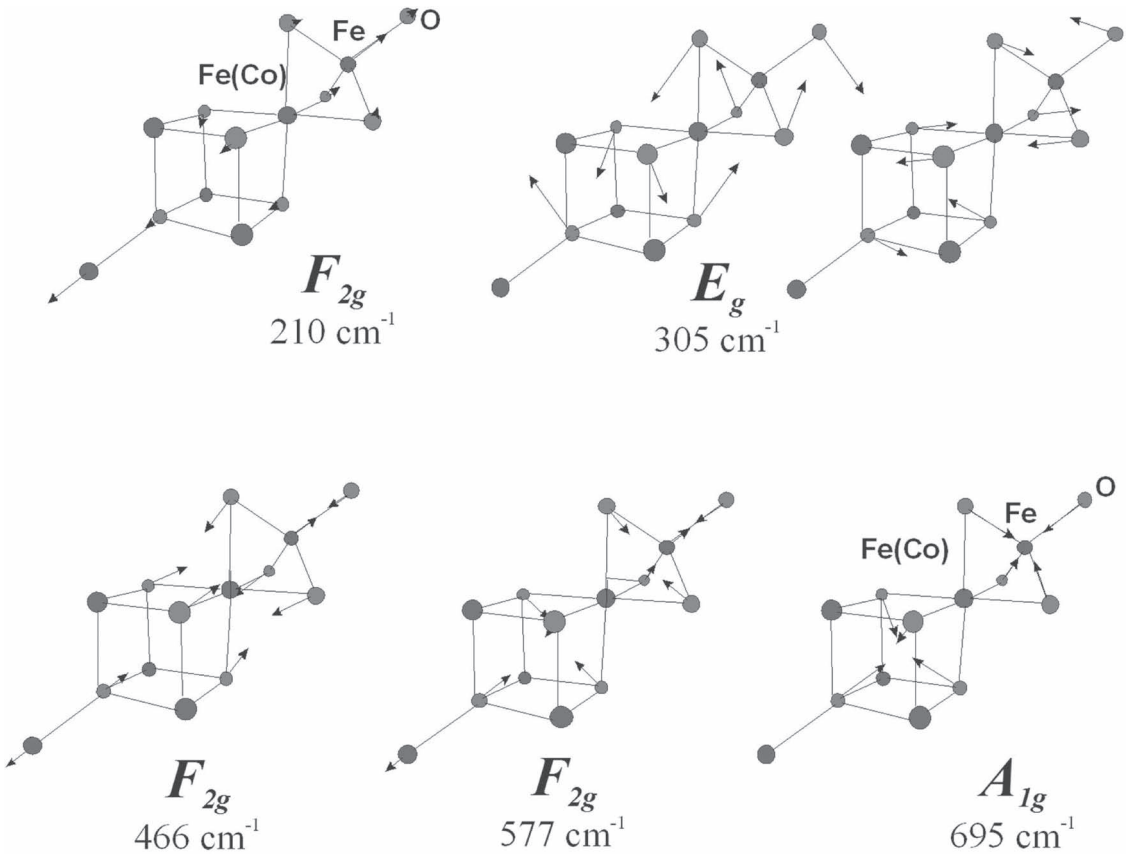

Figure 6. Atomic motions of the Raman active phonon modes for the spinel structure.

it is clear that the, at first sight counterintuitive, increase of ω when expanding the *c*-axis, results from the contribution of the accompanying *a*-axis compression.

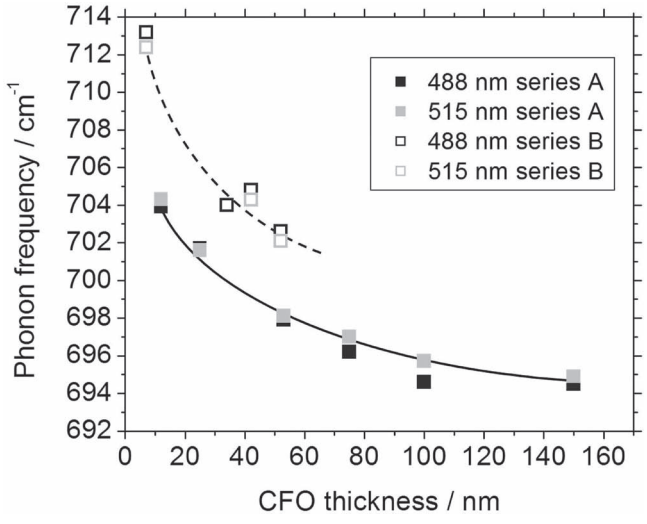

Figure 7. Extracted position of the peak close to 700 cm^{-1} in Raman spectra as shown in Figure 5 as function of the $CoFe_2O_4$ layer thickness. Results using different laser wavelengths are identical. The thickness dependence is monotonous within each samples series "A" and "B" and shows an increase of the phonon frequency for thinner films. Dashed lines are guides to the eye.

Before concluding, it is worth recalling that the Poisson ratio contains rich information on structure and bonding in solids. The atomic packing density (C_g) has been recognized as a fundamental parameter determining ν.[34] For a complex material this can be estimated as $C_g = \rho\sum_i f_i V/\sum_i M_i$ where ρ is the density, M_i is the atomic mass of species i, and f_i and V_i are the corresponding molar fractions and volumes, with $V_i = (4/3)\pi N R_i$, where R_i is the atomic radius and N Avogadro's number. For CFO, $C_g = 0.47$. It is rewarding to notice that according to the Poisson ratio vs. C_g diagram of Rouxel,[34,3] for $C_g = 0.47$ the Poisson ratio should be $\nu \approx 0.2$, or, correspondingly, $\nu^* \approx 0.5$. The agreement between this prediction and our measurements of Figure 4 for CFO grown on MAO is remarkable. The smaller ν^* value determined for CFO films on STO likely results from the higher density of plastic defects that these films should have as a result of their plastic relaxation. Probably, the columnar growth observed for heteroeptaxial growth of spinel oxides on perovskite substrates[35] may also add and contribute to a reduced effective ν^*. In any case, the estimate of $\nu^* \approx 0.5$ on the basis of the atomic packing density (C_g) places CFO deep into the region $\nu > 0$. It thus follows that the spinel structure is dense enough to avoid antirubber-like elastic behavior under epitaxial strain, as confirmed by our exhaustive experimental data.

4. Summary, Conclusions, and Outlook

In summary, we have investigated epitaxial strain effects on the unit-cell deformation and lattice dynamics in $CoFe_2O_4$ thin

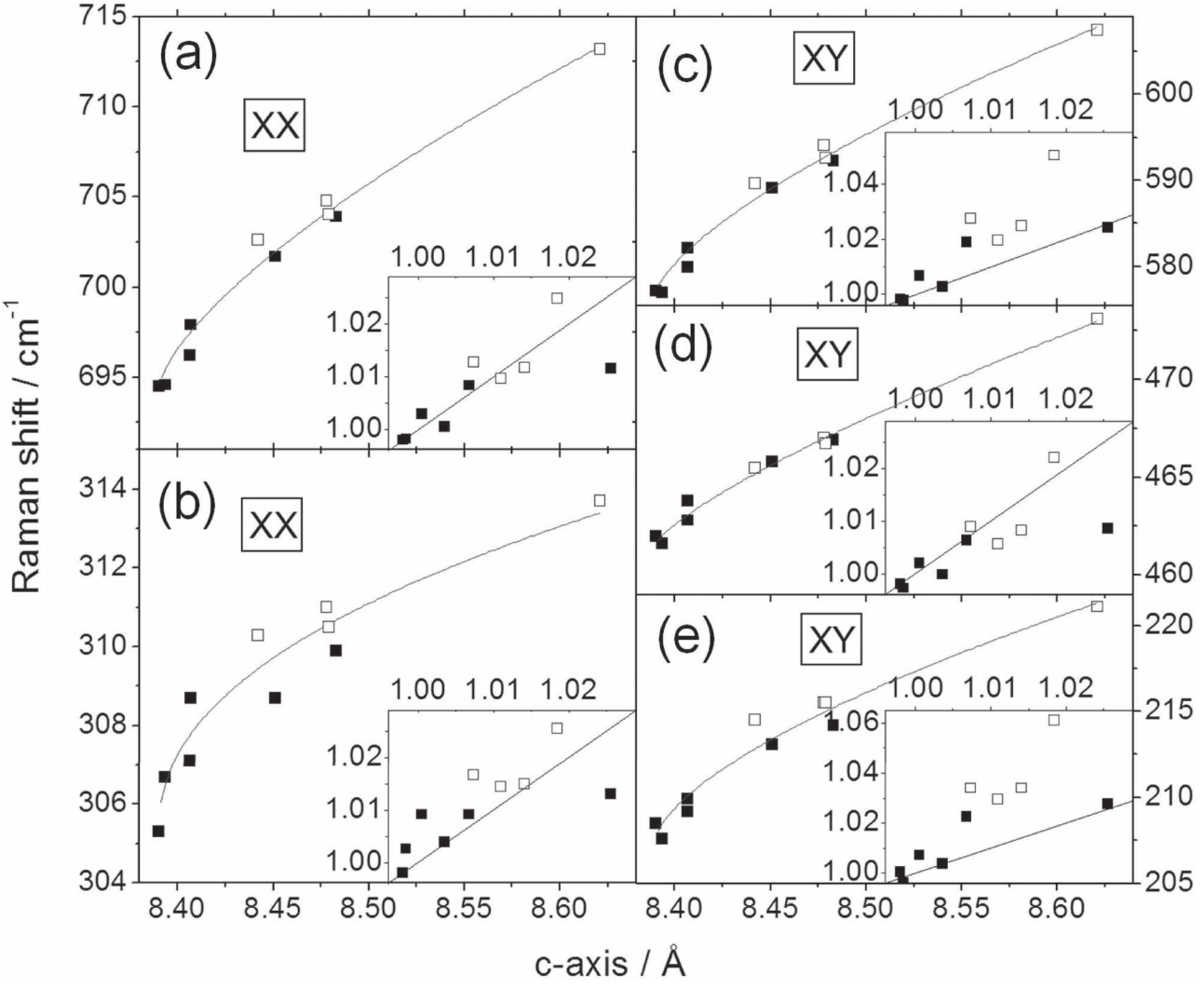

Figure 8. Phonon frequencies ω as extracted from Raman spectra for different modes as a function of the out-of-plane $CoFe_2O_4$ lattice constant determined by X-ray diffraction, corresponding to the different peaks in Figure 5. Data for both series "A" (filled symbols) and "B" (empty symbols) follow the same trend. Lines are fits to the data using the expression $\omega(c) = \omega_0(1 + Z(c - c_0)^{\beta})$. In the insets, the normalized frequencies ω/ω_0 are shown as a function of $(d_0/d)^{3/2}$ where d is the unit cell diagonal length and d_0 its bulk value. For comparison, straight lines corresponding to x = y are shown.

films. This oxide, being representative of a large family of magnetic spinels, displays a rather complex behavior under epitaxial strain. The cell parameters along the load, (bidirectional epitaxial compressive stress) shorten and the transverse cell parameter expands, indicating non-auxetic behavior, while the unit cell volume shrinks. This behavior is in qualitative agreement with recent ab initio calculations, although the measured values are significantly smaller than predictions. In contrast, the measured Poisson ratio is found to be in good accord with expectations based on general arguments of atomic packing density. The dependence of Raman modes on strain can be well understood on the basis of the unit cell volume compression; however, a simple dependence of Raman modes on cell parameters cannot be derived. Theoretical insights are required to achieve a complete description of the strain dependence of Raman spectra.

Table 1. Parameters (Z, β) of the fits $\omega(c) = \omega_0\ (1 + Z(c - c_0))$ describing the variation of the indicated Raman modes on the c-axis length.

Raman mode	Z	β
XX 695 cm^{-1} (A_{1g})	0.075	0.693
XX 305 cm^{-1} (E_g)	0.051	0.448
XY 577 cm^{-1} (F_{2g})	0.148	0.698
XY 466 cm^{-1} (F_{2g})	0.076	0.771
XY 210 cm^{-1} (F_{2g})	0.170	0.643

From a broader perspective, our data show that spinels are non-auxetic, in spite of having a rather open structure and the hinge-like 3D honeycomb bond network recently identified and therefore showing features similar to those of polyacetylene carbon where auxetic behavior was predicted.[19,36] This observation should not be restricted to $CoFe_2O_4$ investigated here,

but should hold for a range of spinel oxides; at least, for those where late transition metal cations with similar ionic radii and bond lengths occupy the characteristic octahedral and tetrahedral cages. On the other hand, anomalous bond compressibility, as measured by the Poisson ratio, should be reflected in functional properties sensitive to interatomic bond lengths and bond angles, particularly superexchange magnetic interactions or even dielectric response. Thus, it could be argued that an auxetic behavior in spinels, as claimed for $CoFe_2O_4$, could lead to an enhanced magnetrostiction (λ)[19] that should be a general characteristic of transition metal spinels. Indeed, $CoFe_2O_4$ has a huge magnetostriction coefficient λ.[37] However, the fact that in spinels λ, although being the largest for $CoFe_2O_4$, is reduced by more than an order of magnitude when the cobalt content is reduced by appropriate substitution,[37] signals that magnetostriction is dominated by the strong spin-orbit coupling of Co^{2+} rather than by anomalous compressive response under load.

Finally, opportunities for auxetic response may still exist if, in the relatively open structure of spinels, the octahedra or tetrahedral polyhedra were loosely filled with smaller cations, either early transition metals or even alkaline ions. Other possibilities are spinel compounds where distinct spins states, thus having distinct orbital symmetry, could compete and vary under load. Alternatively, the characteristic frustration of magnetic interactions and sign-competing magnetic interactions of spinels may lead to complex magnetic orderings that, in presence of strong spin–lattice and/or spin–orbit interactions, may induce the occurrence of structural distortions upon magnetic order and eventually anomalous unit-cell expansion (compression) as recently demonstrated[38] or even auxetic behavior. These considerations could be guiding lines for future research.

Acknowledgements

Financial support by the Spanish Government (Project Nos. MAT2008-06761-C03, MAT2011-29269-C03 and CSD2007-00041), by the Generalitat de Catalunya (Grant No. 2009-SGR-00376), the State of Texas through the Texas Center for Superconductivity at the University of Houston and the Czech Science Foundation (Project P204/11/P339) is acknowledged. The authors are thankful to C. Ederer for useful comments and insights and to F. Rigato for his contribution on the growth of some of the films reported here.

Received: January 27, 2012
Published online: June 13, 2012

[1] J. Glieck, *The New York Times* 14 April **1987**.
[2] J. N. Grima, R. Gatt, V. Zammit, J. J. Williams, K. E. Evans, A. Alderson, R. I. Walton, *J. Appl. Phys.* **2007**, *101*, 086102.
[3] G. N. Greaves, A. L. Greer, R. S. Lakes, T. Rouxel, *Nat. Mater.* **2011**, *10*, 823.
[4] K. E. Evans, M. A. Nkansah, I. J. Hutchinson, S. C. Rogers, *Nature* **1991**, *353*, 124.
[5] R. Baughman, J. M. Shacklette, A. A. Zakhidov, S. Stafström, *Nature* **1998**, *392*, 362.
[6] M. Nakamura, *Mater. Res. Soc. Bull.* **1995**, *20*, 33.
[7] L. Dong, D. S. Stone, R. S. Lakes, *Philos. Mag. Lett.* **2010**, *90*, 23.
[8] J. H. Haeni, P. Irvin, W. Chang, R. Uecker, P. Reiche, Y. L. Li, S. Choudhury, W. Tian, M. E. Hawley, B. Craigo, A. K. Tagantsev, X. Q. Pan, S. K. Streiffer, L. Q. Chen, S. W. Kirchoefer, J. Levy, D. G. Schlom, *Nature* **2004**, *430*, 758.
[9] K. J. Choi, M. Biegalski, Y. L. Li, A. Sharan, J. Schubert, R. Uecker, P. Reiche, Y. B. Chen, X. Q. Pan, V. Gopalan, L.-Q. Chen, D. G. Schlom, C. B. Eom, *Science* **2004**, *306*, 1005.
[10] N. A. Pertsev, A. G. Zembilgotov, A. K. Tagantsev, *Phys. Rev. Lett* **1998**, *80*, 1988.
[11] J. H. Lee, L. Fang, E. Vlahos, X. Ke, Y. W. Jung, L. F. Kourkoutis, J.-W. Kim, P. J. Ryan, T. Heeg, M. Roeckerath, V. Goian, M. Bernhagen, R. Uecker, P. C. Hammel, K. M. Rabe, S. Kamba, J. Schubert, J. W. Freeland, D. A. Muller, C. J. Fennie, P. Schiffer, V. Gopalan, E. Johnston-Halperin, D. G. Schlom, *Nature* **2010**, *466*, 954.
[12] J. Fontcuberta, B. Martínez, A. Seffar, J. L. García-Muñoz, S. Piñol, X. Obradors, *Phys. Rev. Lett.* **1996**, *76*, 1122.
[13] I. C. Infante, F. Sánchez, J. Fontcuberta, M. Wojcik, E. Jedryka, S. Estradé, F. Peiró, J. Arbiol, V. Laukhin, J. P. Espinós, *Phys. Rev. B* **2007**, *76*, 224415.
[14] J. Fontcuberta, I. Fina, L. Fàbrega, F. Sánchez, X. Martí, V. Skumryev, *Phase Trans.* **2011**, *84*, 555.
[15] Y. Suzuki, G. Hu, R. B. Van Dover, R. J. Cava, *J. Magn. Magn. Mater.* **1999**, *191*, 1.
[16] A. Lisfi, C. M. Williams, L. T. Nguyen, J. C. Lodder, A. Coleman, H. Corcoran, A. Johnson, P. Chang, A. Kumar, W. Morgan, *Phys. Rev. B* **2007**, *76*, 054405.
[17] S. K. Arora, R. G. S. Sofin, I. V. Shvets, M. Luysberg, *J. Appl. Phys.* **2006**, *100*, 73908.
[18] F. Rigato, J. Geshev, V. Skumryev, J. Fontcuberta, *J. Appl. Phys.* **2009**, *106*, 113924.
[19] M. Valant, A. Axelsson, F. Aguesse, N. M. Alford, *Adv. Funct. Mater.* **2010**, *20*, 644.
[20] A. K. Axelsson, F. Aguesse, L. Spillane, M. Valant, D. W. McComb, N. Alford, *Acta Mater.* **2011**, *59*, 514.
[21] M. Ziese, arXiv:1103.3666v1 **2011**.
[22] D. Fritsch, C. Ederer, *Phys. Rev. B* **2010**, *82*, 104117.
[23] a) U. Lüders, A. Barthelemy, M. Bibes, K. Bouzehouane, S. Fusil, E. Jacquet, J. P. Contour, J.-F. Bobo, J. Fontcuberta, A. Fert, *Adv. Mater.* **2006**, *18*, 1733; b) U. Lüders, M. Bibes, K. Bouzehouane, E. Jacquet, J.-P. Contour, S. Fusil, J. F. Bobo, J. Fontcuberta, A. Barthelemy, A. Fert, *Appl. Phys. Lett.* **2006**, *88*, 082505.
[24] A. V. Ramos, M.-J. Guittet, J.-B. Moussy, R. Mattana, C. Deranlot, F. Petroff, C. Gatel, *Appl. Phys. Lett.* **2007**, *91*, 122107.
[25] Y. F. Chen, M. Ziese, *Phys. Rev. B* **2007**, *76*, 014426.
[26] A. Ramos, T. Santos, G. Miao, M. Guittet, J. Moussy, J. Moodera, *Phys. Rev. B* **2008**, *78*, 180402.
[27] Y. K. Takahashi, S. Kasai, T. Furubayashi, S. Mitani, K. Inomata, K. Hono, *Appl. Phys. Lett.* **2010**, *96*, 072512.
[28] F. Rigato, S. Piano, M. Foerster, F. Giubileo, A. M. Cucolo, J. Fontcuberta, *Phys. Rev. B* **2010**, *81*, 174415.
[29] M. Foerster, D. F. Gutierrez, F. Rigato, J. M. Rebled, F. Peiro, J. Fontcuberta, *Appl. Phys. Lett.* **2010**, *97*, 242508.
[30] J. Y. Tsao, *Materials Fundamentals of Molecular Beam Epitaxy*, Academic Press, London **1993**.
[31] Z. Li, E. S. Fisher, J. Z. Liu, M. N. Nevitt, *J. Mater. Sci.* **1991**, *26*, 2621.
[32] V. G. Ivanov, M. V. Abrashev, M. N. Iliev, M. M. Gospodinov, J. Meen, M. I. Arroyo, *Phys. Rev. B* **2010**, *82*, 024104.
[33] M. N. Iliev, D. Mazumdar, J. X. Ma, A. Gupta, F. Rigato, J. Fontcuberta, *Phys. Rev. B* **2011**, *83*, 014108.
[34] T. Rouxel, *J. Am. Ceram. Soc.* **2007**, *90*, 3019.
[35] M. Foerster, J. M. Rebled, S. Estradé, F. Sánchez, F. Peiró, J. Fontcuberta, *Phys. Rev. B* **2011**, *84*, 144422.
[36] R. H. Baughman, D. S. Galvão, *Nature* **1993**, *365*, 735.
[37] R. M. Bozorth, E. F. Tilden, A. J. Williams, *Phys. Rev.* **1955**, *99*, 1788.
[38] J. Hemberger, H.-A. Krug von Nidda, V. Tsurkan, A. Loidl, *Phys. Rev. Lett.* **2007**, *98*, 147203.